29 May 2010, 9:30 am - 10:00 am

Liquefaction, Screening, and Remediation of Silty Soils

S. Thevanayagam

University at Buffalo, SUNY Buffalo, NY


Fifth International Conference on
Recent Advances in Geotechnical Earthquake Engineering and Soil Dynamics
and Symposium in Honor of Professor I.M. Idriss
May 24-29, 2010 • San Diego, California

LIQUEFACTION, SCREENING, AND REMEDIATION OF SILTY SOILS

S. Thevanayagam
University at Buffalo, SUNY
Buffalo, NY 14260

ABSTRACT

Assessing liquefaction potential, in situ screening, and remediation of non-plastic silty soils are difficult problems. Presence of silt particles among the sand grains in silty soils affects the soil response in each of the above cases in different ways. First part of this paper addresses the effects of silt content on liquefaction resistance, hydraulic conductivity, and coefficient of consolidation of silty soils compared to clean sand. Secondly it addresses the effects of silt content and consolidation characteristics on cone resistance of silty soils and sand. A relationship between normalized cone resistance, liquefaction resistance, and consolidation characteristics is presented. The third part of the paper focuses on the effects of silt content and soil permeability on the effectiveness of dynamic compaction (DC) and vibratory stone column (SC) supplemented with wick drains to densify silty soils and mitigate liquefaction..

INTRODUCTION

Current liquefaction screening techniques rely on knowledge from extensive laboratory research conducted on liquefaction resistance of clean sands and field performance data during past earthquakes. Field observations have been documented in the form of normalized penetration resistance (SPT $(N_1)_{60}$, CPT q_{c1N}) (Seed et al. 1983, Youd and Idriss 2001, Robertson and Wride 1997), and shear wave velocity (v_{s1}) (Andrus and Stokoe, 2000) versus cyclic stress ratio (CSR=τ/σ'_{vo}) induced by the earthquakes, corrected for magnitude, for many sites. Cyclic resistance ratio (CRR), applicable for a standard earthquake magnitude of 7.5, of a soil deposit with a known value of q_{c1N} is obtained from a demarcation line drawn between the field-observation-based data points which correspond to liquefied sites and those that did not liquefy in Fig.1. The CRR determined in this manner depends on fines content of the soil for a given q_{c1N}. This has sparked numerous research on the effects of fines on cyclic resistance of silty sands (e.g. Chang et al. 1982, Kuerbis et al. 1988, Vaid 1994, Koester 1994, Zlatovic and Ishihara 1997, Polito and Martin 2001). Results show that silt content affects liquefaction resistance of silty soils compared to sand at the same void ratio. More recent studies also show that silt content also significantly affects permeability, compressibility, and consolidation characteristics of silty sands compared to sand (Thevanayagam et al. 2001). The latter characteristics could influence penetration resistance as well. Two soils with the same stress-strain characteristics and liquefaction resistance but with different silt contents may have different permeability, compressibility, and coefficients of consolidation. Their cone resistance could be different due to different degrees of partial drainage, which may occur around the cone during penetration in each soil. A unique correlation between cyclic liquefaction resistance and penetration resistance may not be possible without considering the effects of fines, viz. coefficient of consolidation, on penetration resistance (Thevanayagam and Martin 2002, Thevanayagam et al. 2003, Thevanayagam and Ecemis 2008). A correlation between cyclic resistance, cone resistance, compressibility and permeability characteristics may be possible.

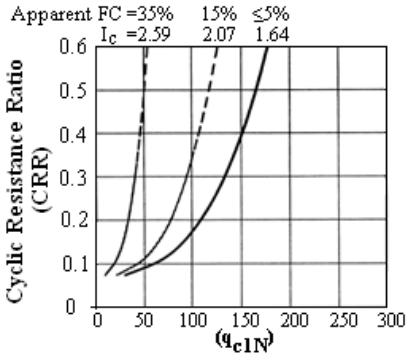

Fig.1 Field Liquefaction Screening Charts –CPT (Youd et al. 2001, Robertson and Wride 1997)

Densification techniques such as dynamic compaction (DC) and vibro-stone column (SC) are among the most field proven and commonly used techniques for liquefaction mitigation in sands (Figs. 2a and c). The DC technique involves high-energy impacts to the ground surface by systematically dropping heavy weights of 5 to 35 Mg from heights ranging from 10 to 40 m to compact the underlying ground using heavy crawler cranes (Lukas 1995). Vibro-stone column installation (FHWA 2001) process involves insertion of a vibratory probe with rotating eccentric mass and power rating in the vicinity of 120kW. The probe plunges into the ground due to its self-weight and vibratory energy, which facilitates penetration of the probe. Once the specified depth (depth of stone column) is reached, the probe is withdrawn in steps (lifts) of about 1m. During withdrawal of the probe, the hole is backfilled with gravel. During each lift the probe is then reinserted expanding the stone column diameter. This process is repeated several times until a limiting condition is achieved. Densification of silty sand deposits containing high silt contents appears to be feasible only when these techniques are supplemented with wick drains (Figs. 2 b and d) (Dise et al. 1994, Han 1998, Luehring et al. 2001). Traditionally, field design of these approaches rely on site specific field pilot trials and/or past experience based on case histories (Lukas 1995, Baez 1995). In the case of silty soils case histories are scarce. More recently advances have been made that enable detailed analyses of site response and changes in soil densities during DC and SC installations with due consideration for the influence of soil conditions including effects of silt content and soil permeability (Shenthan 2006, Nashed 2006). These advances allow a study of the effects of wick drains, spacing between wick drains, soil permeability, impact grid pattern and impact energy in the case of DC and diameter and spacing of stone columns in the case of SC on the degree of soil densification improvement achievable in the field, and select optimum field operation parameters for DC and SC for a site.

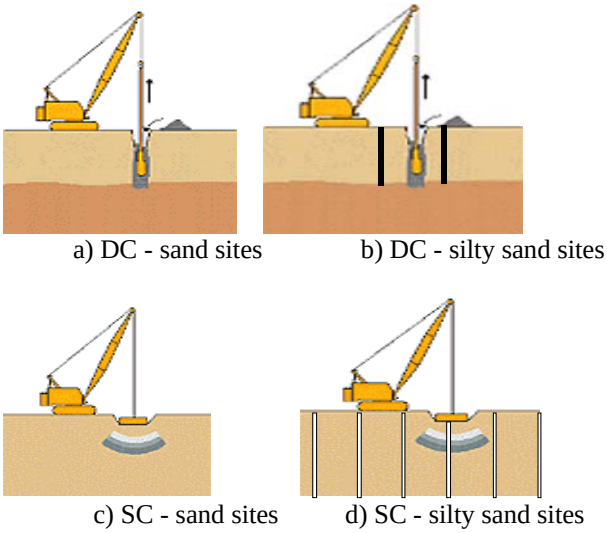

a) DC - sand sites b) DC - silty sand sites

c) SC - sand sites d) SC - silty sand sites

Fig. 2 Dynamic compaction and Vibro-stone columns with and without wick drains

This paper presents a summary of these advances on understanding of the influences of fines on undrained cyclic resistance and cone penetration resistance of silty soils, and effectiveness of dynamic compaction and stone columns supplemented with pre-installed wick drains for liquefaction mitigation of silty sands. A revised liquefaction-screening chart that takes into account the effects of consolidation characteristics on penetration resistance is presented. Simplified design charts for stone columns and dynamic compaction are also presented.

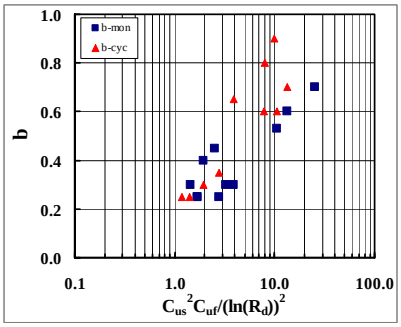

(a) parameter b

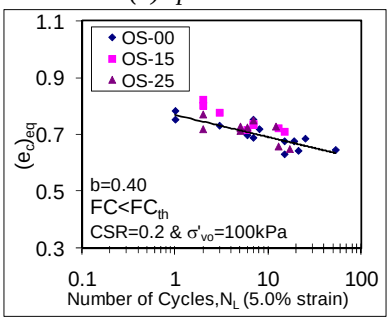

(b) liquefaction resistance

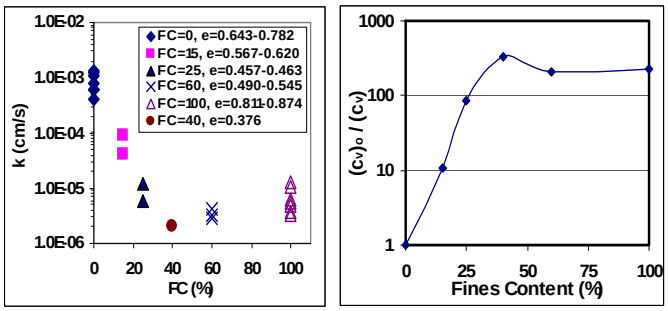

(c) hydraulic conductivity k (d) coeff. of consolidation ratio

Fig.3 Effect of non-plastic fines content

EFFECTS OF FINES CONTENT

Soil Properties

Liquefaction Resistance: A large data set is now available in the literature on the effects of non-plastic fines content on undrained cyclic resistance of silty soils. Generally, at the same void ratio, the cyclic resistance decreases with an

increase in silt content up to a threshold value of fines content (fc_{th}); cyclic resistance increases thereafter with further increase in silt content. At the same equivalent void ratios $(e_c)_{eq}=[e+(1-b)fc]/(1-(1-b)fc)]$ or $(e_f)_{eq}=[e/(fc+(1-fc)/R_d^m)]$, at silt content (fc) less than fc_{th} or more than fc_{th}, respectively, a silty sand and sand have nearly the same cyclic resistance; where fc = fines content by weight, R_d= ratio of the d_{50}'s of the host sand and silt in the soil mix, and b and m are constants depending on grain size characteristics such as uniformity coefficient of coarse grain soil (C_{us}) and fine grained soil (C_{uf}) in the soil mix (Thevanayagam 2007a,b). Fig.3a shows an approximate relationship between b and (R_d, C_{us} and C_{uf}). Fig. 3b shows an example relationship for undrained cyclic resistance of Ottawa sand-silt mixes prepared at silt content up to 25% plotted against $(e_c)_{eq}$. Such a relationship also holds for undrained shear strength, stress-strain characteristics, shear modulus and shear wave velocity as well (Thevanayagam and Liang 2001, Ni et al. 2004).

k and c_v: Although there is reasonable correlation between the cyclic resistance, undrained strength, shear modulus, and shear wave velocity and equivalent void ratio $(e)_{eq}$, hydraulic conductivity k of silty soils is significantly affected by silt content rather than by $(e)_{eq}$. Fig.3c shows the effect of fines content on k for Ottawa sand-silt mixes (Thevanayagam et al. 2001). Fig.3d shows the normalized (c_{vo}/c_v) at nearly the same $(e)_{eq}$ versus silt content, where c_v and c_{vo} are the coefficients of consolidation of Ottawa sand-silt mix and clean Ottawa sand, respectively. Both k and c_v decrease with increasing silt content. This indicates that a silty sand and sand at the same $(e)_{eq}$ may have the same cyclic resistance but they may exhibit very different k and c_v.

Penetration Resistance

Consider penetration of a CPT cone into a saturated sand or silty sand. The penetration causes highly non-uniform shear strain and excess pore pressures around the cone. A sand and a silty sand with the same stress-strain behavior and undrained cyclic resistance but different k and c_v, depending on the rate of penetration and cone size, may experience different degrees of partial dissipation of excess pore pressures and consolidation around the cone during penetration. Therefore the normalized penetration resistance q_{c1N} may differ for these two soils, unless the penetration is very slow allowing fully drained conditions or too fast to allow fully undrained conditions to prevail. Under standard penetration rate of 2 cm/s (ASTM D3441), neither fully drained nor fully undrained conditions may prevail in all soils.

Numerical Simulation: The influence of k and c_V on possible differences in partial drainage conditions that may prevail around a cone tip during cone penetration and its influence on cone penetration resistance of sand and silty soils was studied using finite element numerical simulation study using finite element code ABAQUS (2000) (Fig.4). The soil was simulated using Drucker-Prager model. A vertical effective stress of 100 kPa was imposed near the cone to simulate the cone at a depth with nearly 100 kPa effective vertical stress. The soil was fully saturated. The diameter d of the cone was 4.37cm, and the cone tip was placed at 36cm from the top surface of the finite element mesh. The mesh extended to a distance of 54cm (about 15d) below the cone tip and 40 cm away horizontally (about 18d) from the cone axis (Ecemis 2008). Such large distances were chosen to reduce the boundary effects. On the bottom and two vertical sides, the normal component of displacement and fluid flow were fixed at zero. No pore fluid flow was permitted across cone body. Material properties, including dilation angles, required for numerical simulation of cone penetration were obtained from several sets of triaxial test data on Ottawa sand and sand-silt mixes for a wide range of relative densities characterized by $(D_{rc})_{eq}$ (Ecemis 2008, Thevanayagam et al. 2003). $(D_{rc})_{eq}$ has been defined as $(D_{rc})_{eq}=[e_{max,HS}-(e_c)_{eq}]/[e_{max,HS}-(e_{min,HS})]$, where $e_{max,HS}$ = maximum void ratio of the host sand, $e_{min,HS}$ = minimum void ratio of the host sand. Pore pressure responses and cone penetration resistances were monitored while the cone was penetrated at a constant rate v=2 cm/s. In each case, several parametric simulations were also done by varying k.

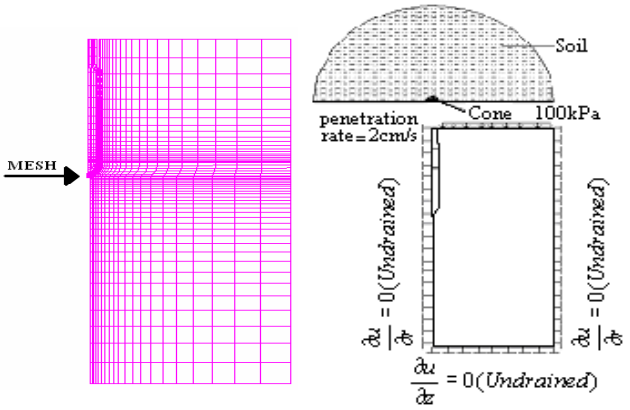

Fig.4 Finite element mesh – CPT model

Effect of k and c_v on q_{c1N}: Figs.5a-c show the effect of permeability on the excess pore water pressures around the cone for a medium-dense soil at $(D_{rc})_{eq}$=58% for three different k values. Fig.6a shows the normalized excess pore pressure at the tip of the cone plotted against a normalized penetration rate ($T=vd/c_v$) and equivalent relative density $(D_{rc})_{eq}$. Fig.6b shows the normalized cone resistance, q_{c1N} plotted against T and $(D_{rc})_{eq}$. Both, the excess pore pressures and q_{c1N} for a given $(D_{rc})_{eq}$ depend on consolidation characteristics parameter T. For loose soils, the excess pore pressure at the cone tip steadily increases with an increase in T. Beyond a value of T in the range of about 5 to 10, the excess pore pressure ratio reaches a high value and remains little affected by any further increase in T, indicating nearly undrained penetration. Similarly, at values of T less than about 0.05 to 0.01, the excess pore pressure is small and is little affected by any further decrease in T, indicating a highly

drained condition around the cone. A partially drained condition prevails at intermediate T values of about 5 to 0.01. In the case of dense soils, the excess pore pressure is small for T values less than about 0.05 to 0.01, indicating drained soil response during cone penetration. At high values of T in the range of about 5 to 10, the excess pore pressure is negative and remains unaffected by further increase in T. This is indicative of highly dilative response of the soil and undrained conditions around the cone. For intermediate values of T, the excess pore pressure is affected by T, indicating existence of partial drainage effects around the cone tip. The q_{c1N} at the cone tip steadily decrease with an increase in T as shown in Fig.6b. For each case, beyond a value of T in the range of about 5 to 10, the q_{c1N} reaches a low value and remains little affected by further increase in T, indicating nearly undrained penetration. Similarly at values of T less than about 0.05 to 0.01 the q_{c1N} is high and is little affected by further decrease in T, indicating a highly drained condition around the probe. A partially drained condition prevails at intermediate T values of about 5 to 0.01. These effects are reflected in the normalized cone penetration resistance in Fig.6b. Observations from Fig.6 imply that, q_{c1N} for a low permeable silty sand would be smaller than that of highly permeable clean sand at the same $(D_{rc})_{eq}$. This difference is attributable to the presence of fines, which causes low k and c_v and undrained or partially drained conditions during penetration in silty sands leading to a decrease in tip resistance compared to highly permeable sand.

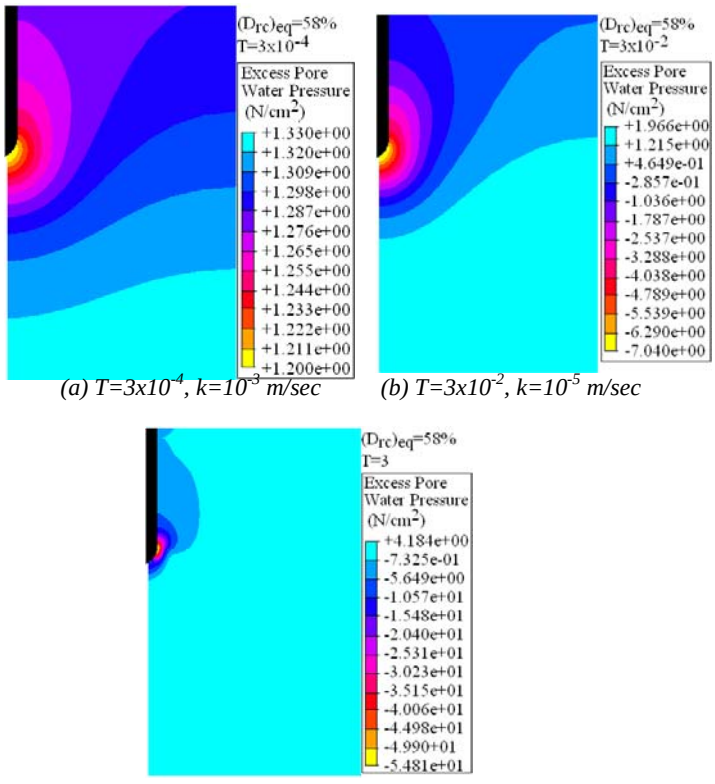

(a) T=3x10^{-4}, k=10^{-3} m/sec *(b) T=3x10^{-2}, k=10^{-5} m/sec*

(c) T=3, k=10^{-7} m/sec

(Dilation angle = 13 degrees; T = vd/c$_v$)

Fig.5 Excess pore pressure response around cone

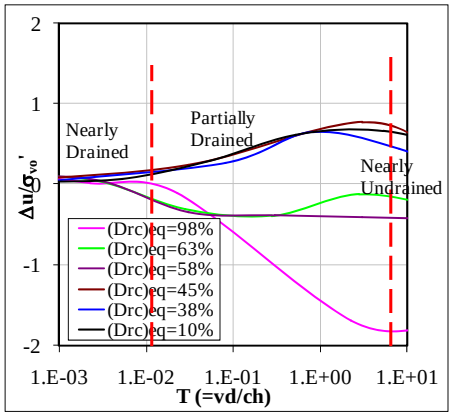

(a) $\Delta u/\sigma'_{vo}$ versus T

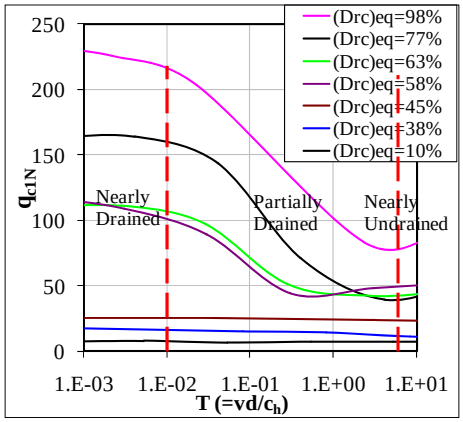

(b) q_{c1N} versus T

Fig.6 Excess pore pressure and q_{c1N}

Liquefaction screening

The q_{c1N} values obtained from the above numerical simulations for each soil at a range of distinct $(D_{rc})_{eq}$ values were also plotted against the corresponding undrained cyclic resistance ratio (CRR) required to cause liquefaction in 15 cycles for that soil at the corresponding $(D_{rc})_{eq}$ obtained from laboratory undrained cyclic triaxial compression tests (Thevanayagam et al. 2003). The solid points in Fig.7a shows this relationship for q_{c1N}-$(CRR)_{TX}$. Based on these numerical data points and additional parametric studies where k was varied for each soil, a generic relationship for q_{c1N} versus $(CRR)_{TX}$ was obtained. This is shown by solid lines. Each solid line refers to a narrow range of T values.

The relationship shown in Fig.7a was further modified to obtain $(CRR)_{field\text{-}7.5}$ applicable for an earthquake of magnitude 7.5 by correcting the $(CRR)_{TX}$ for 15 cycles using the relationship between $(CRR)_{field}$ and $(CRR)_{TX}$ proposed by Castro (1975) and Seed et al. (1978). The $(CRR)_{field\text{-}7.5}$ versus q_{c1N} relationship is shown in Fig.7b. Fig.7b also compares this relationship with the CPT based liquefaction screening chart

proposed by Robertson and Wride (1997), corresponding to nearly clean sands, silty sands at nearly 15% silt content and 35% silt content, respectively. The curves for T<0.006 tend to follow the R-W curves for clean sands. The curves corresponding to 0.02<T<0.06 tend to follow the R-W curve for 15% silt content. The remaining curves tend to follow the R-W curve for 35% silt content. The right and left boundary curves in Fig.7 represent nearly fully drained and nearly undrained penetrations, respectively.

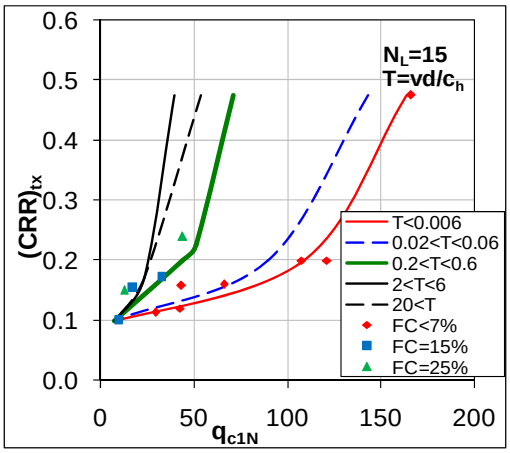

(a) $(CRR)_{tx}$ versus q_{c1N}

(b)

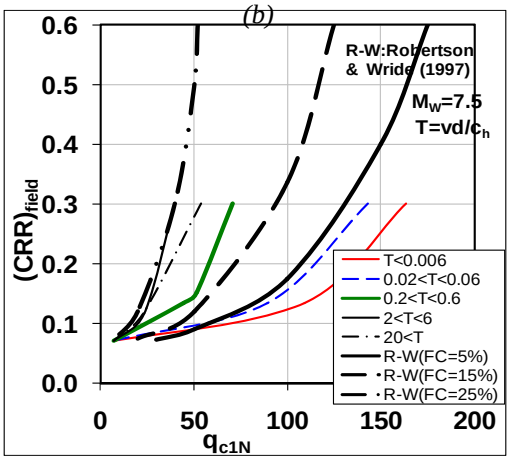

(b) $(CRR)_{feild}$ versus q_{c1N}

Fig.7 Liquefaction Resistance, q_{c1N} and T

The comparison in Fig.7b shows the influence of silt content (viz. k and c_v) on the relationship between cyclic resistance and q_{c1N}. Although the T-dependent q_{c1N}-CRR relationships depict the same trend as observed in the field-based liquefaction screening procedures, additional numerical and physical simulation or field verification studies are needed to validate and refine this trend.

REMEDIATION OF SILTY SOILS

Soil Response During DC and SC

Soil response during dynamic compaction (DC) and stone column (SC) installation involves complex processes. Modeling of these processes and developing analytical tools to assess the increase in soil density, resistance to liquefaction, and cone resistance due to DC and SC are even more complex. The following sections present a simplified approach to model these processes and the results from such analyses.

Excess pore pressure generation and liquefaction in saturated granular soils is a process involving energy dissipation due to friction along grain contacts during cyclic loading, leading to contact slips and concurrent increase in excess pore pressures. The energy required to reach a certain level of pore pressure or cause liquefaction depends primarily on the density of packing and effective confining stress. The magnitude of induced excess pore pressure depends on the cumulative energy dissipated per unit volume of soil, soil density, and confining stress (Berrill and Davis 1985, Figueroa et al. 1994, Thevanayagam et al. 2000, Kayen and Mitchell 1997, Green and Mitchell 2004). If the energy dissipated in a saturated loose granular soil due to vibratory tamping, such as DC, or vibratory stone column installation approaches or exceeds the energy required to cause liquefaction, pore pressure in localized zones around the impact area increases. Soil density increases during dissipation of excess pore pressures (Figs. 8a and b). During the vibratory process, the energy delivered at the vibratory source generates body waves and Rayleigh waves. As these waves radiate and spread through the soil deposit causing vibrations of soil grains, the intensity of energy decays due to geometric radiation due to spreading and loss due to material damping. The energy loss due to material damping causes rise in excess pore pressures. The induced pore pressures are high near the impact zone and decreases with distance from the impact zone. In the case of sands, the permeability of the soil may be large enough for rapid dissipation of the excess pressures. In the case of silty sands supplemented with wick drain, these wick drains facilitate dissipation of excess pore pressures. In both cases, due to repeated vibratory applications, pore pressures increase and dissipate cyclically, and the soil density and the lateral confining stresses around the impact zones increase, resulting in an increase in resistance to liquefaction as well as cone resistance.

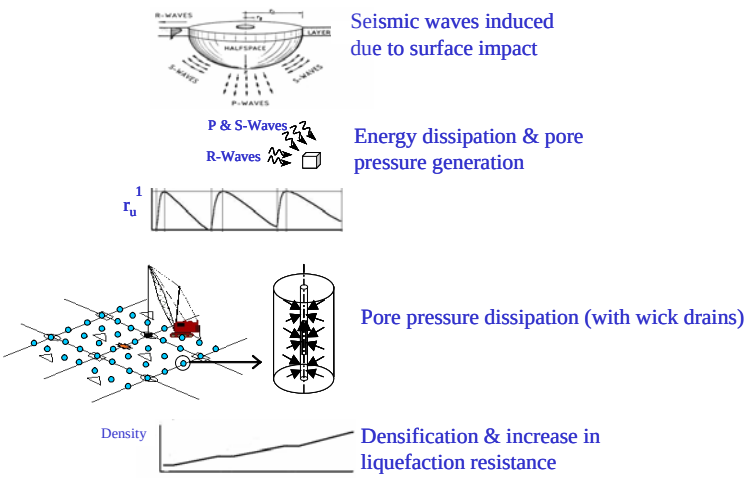

(a) Dynamic Compaction

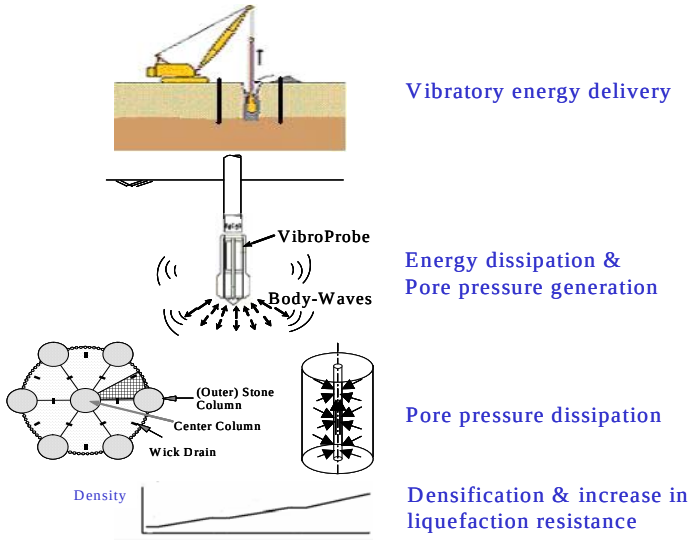

(b) Vibrostone colums

Fig. 8 Soil response during dynamic compaction and stone column installation, supplemented with wick drains

Numerical Simulation of DC and SC

Based on energy principles governing pore pressure generation, simple models for energy dissipation in soils during DC and SC, and consolidation theory a set of numerical simulation models have been developed to simulate the performance of soil deposits and determine density changes, and increase in liquefaction resistance and cone resistance due to DC and SC (Shenthan 2006, Nashed 2006, Thevanayagam et al. 2006, Thevanayagam et al. 2009). Simple attenuation relationships were used to estimate the spatial distribution of energy dissipated in the soil during DC and SC. Experimental data based on energy principles was used to estimate the spatial distribution of field pore pressures generated by DC and SC based on energy dissipated in the soil. Coupled consolidation equations were used to simulate soil consolidation to determine post-improvement soil density profiles. The influence of non-plastic fines content was taken into account in this simulation model by considering their effects on liquefaction resistance as well as on compressibility and hydraulic conductivity.

Dynamic Compaction

Several parametric studies were conducted, using the above simulation approach, to study the effects of k, wick drain spacing S_w and diameter d_w, impact grid spacing S, impact energy WH, number of impacts per grid point, and number of passes on the effective depth of influence d_{max} feasible by dynamic compaction as well as to determine post-improvement density profile. The cumulative energy applied at the simulation sites ranged from 100 to 300 Mg.m/m^2. In each case, the soil profile at the site was considered to be uniform loose soil with initial equivalent normalized SPT blow count of $(N_1)_{60cs}$ of 7.5 (Nashed 2006, Thevanayagam et al. 2006). The groundwater was assumed to be at 2 m below the ground surface. The impact grid pattern for silty sand sites was assumed as shown in Fig. 9, with S=15.2 m. Each grid point received a total of 12 impacts. The time cycle t_o between any two consecutive impacts was selected as 2 minutes. k was varied in the range of 10^{-7} to 10^{-8} m/s to represent the effect of different amounts of silt content. S_w was varied from 1 to 2 m. The equivalent diameter of the wick drains was 5 cm. Although most of the studies for silty soil site included presence of pre-installed wick drains, for comparative analyses purposes a few simulations were also conducted assuming presence of no pre-installed drains using an impact grid pattern shown in Figure 10. Effective depth of influence of dynamic compaction d_{max} was determined at a location midway between primary and secondary impact locations.

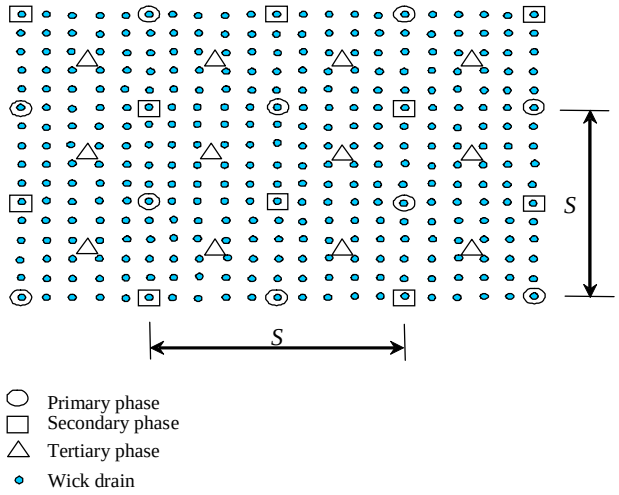

Fig. 9. Typical impact grid pattern with wick drains

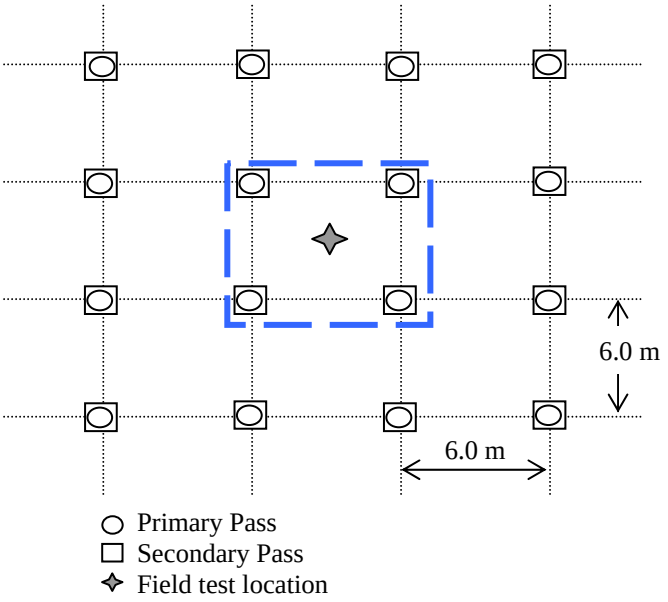

Fig. 10. Typical impact grid pattern without wick drains

The studies for clean sand sites were done without pre-installed wick drains using the grid pattern shown in Fig. 10, with S= 6 m. Each grid point received a total of 8 impacts. k was set in the range of 10^{-5} to 10^{-6} m/s, representing fine sand. The d_{max} was determined at the center of the square impact grid pattern.

Effect of k on d_{max} – without Wick Drains: Fig. 11 shows the results for d_{max} versus WH for clean sand, using grid pattern shown in Fig. 10, without pre-installed wick drains. The empirical relationship for d_{max} ($=n(WH)^{0.5}$ for sands with n=0.5, Lukas 1995) is also shown in this figure. The numerical simulations are in close agreement with the empirical relationship. The numerical simulations for silty soil sites, without pre-installed wick drains, with k less than 10^{-6} m/s showed little or no improvement using grid pattern in Figure 10. Therefore further simulations were not carried out.

Effect of k on d_{max} – with Wick Drains: Fig. 12 shows the relationship between d_{max} and WH for silty sands with wick drain spaced at 1.5 m for two different values of k. The empirical relationship for d_{max} ($=0.5(WH)^{0.5}$) for highly permeable sand sites is also superimposed in this figure. The results show that, when closely spaced wick drains are present, d_{max} increases with WH. d_{max} increases with an increase in k and approaches that of sands. The results show that silty soils with k values as low as 10^{-7} m/s to10^{-8} m/s may be improved by dynamic compaction provided that pre-installed wick drains are present.

Effect of Drain Spacing on d_{max}: Figs. 13 and 14 show the effect of wick drain spacing on d_{max} for a silty soil deposit with k of 10^{-7} m/s and pre-improvement $(N_1)_{60cs}$ of 7.5. As the drain spacing gets closer, the tributary area covered by the drains become smaller and the drains become more effective in dissipating the excess pressures during DC installation. This extends the depth of influence of dynamic compaction.

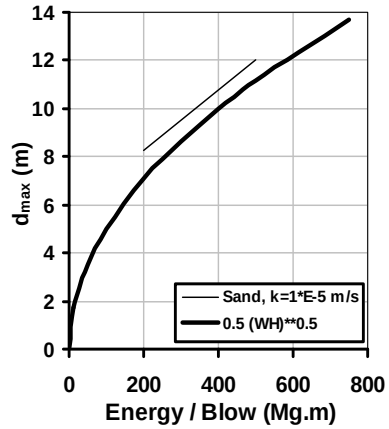

Fig. 11. Clean sand site without wick drain, $(N_1)_{60cs}$ = 7.5

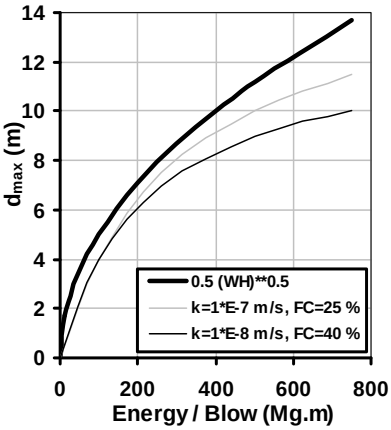

Fig. 12. Silty sand site with wick drain, $(N_1)_{60cs}$=7.5, S_w=1.5m

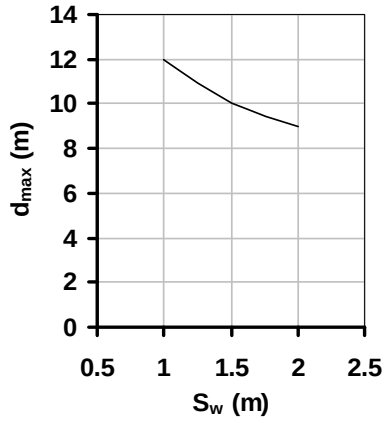

Fig. 13. Effect of wick drains spacing on d_{max} (silty sand site) (WH=500 Mg.m, k=10^{-7}m/s, $(N_1)_{60cs}$=7.5, S_w=1.5m)

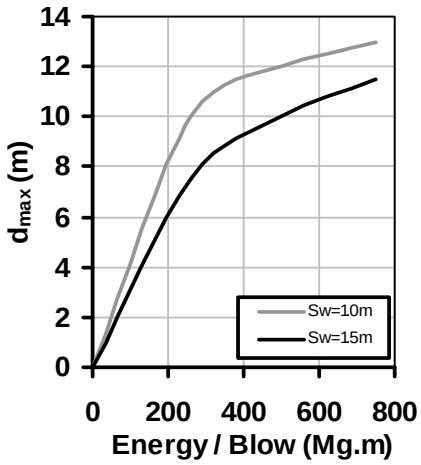

Fig. 14. Effect of k on d_{max} ($k=10^{-7}$ m/s, $(N_1)_{60cs}=7.5$)

Pre- and Post-DC Profile: Several additional numerical simulations were conducted to obtain a relationship between pre- and post-dynamic compaction densities for various uniform silty soil sites, pre-installed with wick drains. For all simulations, the impact grid pattern was assumed to be as shown in Fig.9. Each simulation included three phases of impact, primary, secondary, and tertiary, respectively, at the grid locations shown in Fig.9. The energy per impact (*WH*), impact grid spacing *S*, total number of impacts per grid point during each phase (N_I), wick drain spacing S_w, wick drain size d_w, and time cycle between impacts t_o were varied for each simulation. Groundwater level was assumed to be at 2.0 m depth from impact surface. After each simulation, the density profiles were converted to $(N_1)_{60cs}$ (Nashed 2006, Thevanayagam et al. 2006, 2009).

Two sets of results are presented in Figs. 15 and 16. For these examples, d_w= 5 cm and S_w=1.5m. Wick drains were pre-installed in a rectangular pattern. The number of impacts per grid location and the time cycle between impacts were set at N_I = 12 and t_o = 2 min., respectively. Fig. 15 shows the pre- and post-improvement $(N_1)_{60cs}$ profiles for two uniform soil deposits with pre-improvement $(N_1)_{60cs}$=7.5 and 16, respectively and impact grid spacing of S=15 m. Figs.15a-b are for k =10^{-7} m/s, and Figs. 15c-d are for and k =10^{-8} m/s. Each curve in these figures show the pre-improvement profile and post improvement profiles, respectively, for a different energy per impact *WH* of 100, 250, 500, and 750 Mg.m, respectively. Fig. 16 is for impact grid spacing of *S* = 12 m and energy per impact *WH* of 100, 250, and 500 Mg.m, respectively. The improved soil profiles follow a pattern similar to those observed in field case histories. Comparisons of simulation results for specific case histories are presented elsewhere (Nashed et al. 2009a-b).

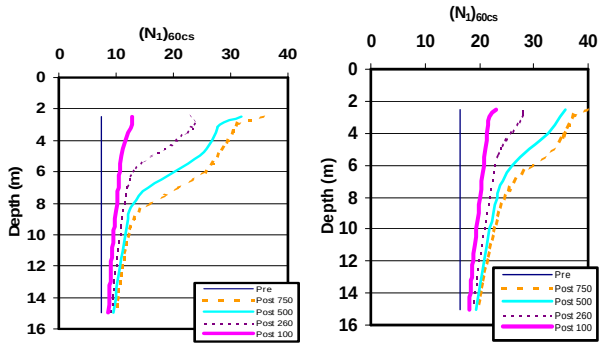

a) $k=10^{-7}$m/s, pre-$(N_1)_{60cs}$=7.5 b) $k=10^{-7}$m/s, pre-$(N_1)_{60cs}$=16

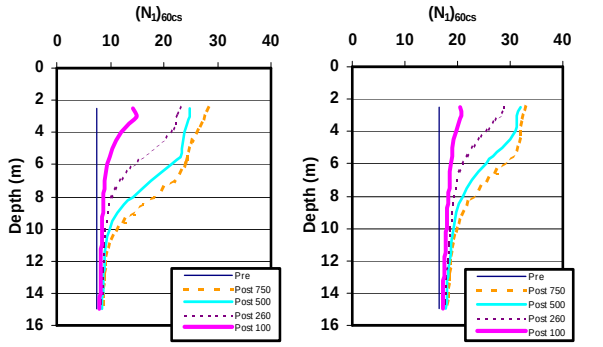

c) $k=10^{-8}$m/s, pre-$(N_1)_{60cs}$=7.5 d) $k=10^{-8}$m/s, pre-$(N_1)_{60cs}$=16

Fig. 15. Pre- and Post-improvement $(N_1)_{60cs}$ for S = 15 m (Post 750: WH = 750 Mg. m)

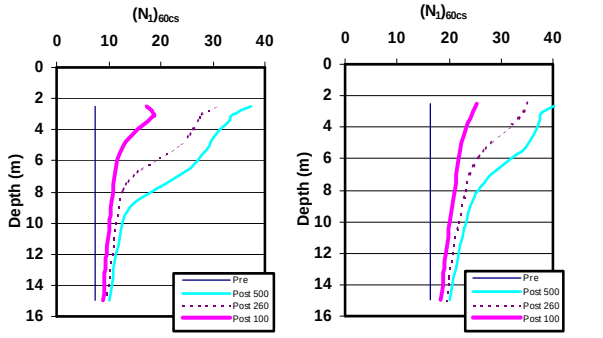

a) $k=10^{-7}$m/s, pre-$(N_1)_{60cs}$=7.5 b) $k=10^{-7}$m/s, pre-$(N_1)_{60cs}$=16

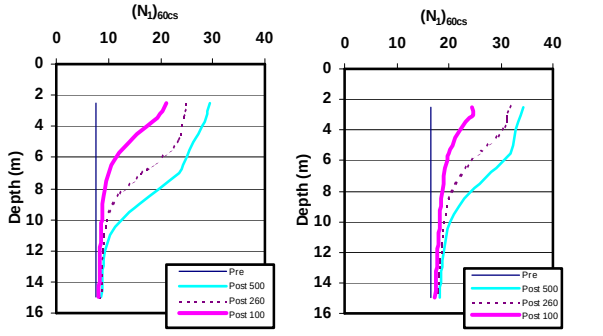

c) $k=10^{-8}$m/s, pre-$(N_1)_{60cs}$=7.5 d) $k=10^{-8}$m/s, pre-$(N_1)_{60cs}$=16

Fig. 16. Pre- and Post-improvement $(N_1)_{60cs}$ for S =12 m (Post 500: WH = 500 Mg. m)

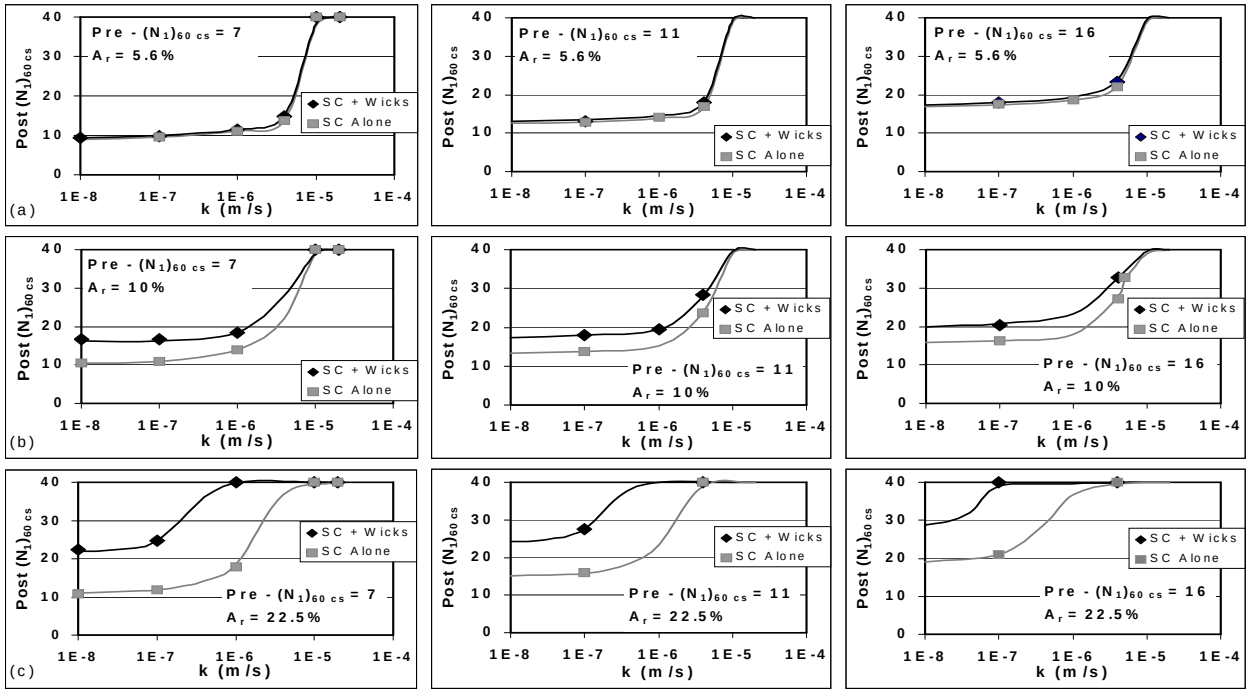

Fig. 17. Vibro-stone columns – Post-Improvement design charts
(SC + Wicks = vibro-stone column with wicks; SC = vibro-stone column without wicks)

Vibrostone Columns

In the case of vibrostone columns, numerical simulations were conducted to obtain the relationship between pre- and post-improvement densities for various uniform soil sites containing clean sands to non-plastic silty soils supplemented with or without wick drains. The diameter of stone columns was set at 0.9 m installed in a triangular pattern. Three different area replacement ratios were considered (A_r = 5.6, 10, and 22.5%). Area replacement is defined as the cross sectional area divided by the tributary area of the soil surrounding each stone column. For all simulations, the power rating of the vibratory probe was set at 120 kW. In cases where supplementary wick drains were considered, the diameter of wick drains was assumed to be 5 cm, pre-installed at midpoints between stone columns. The results for post-improvement density profiles were converted to equivalent normalized clean sand SPT blow counts $(N_1)_{60cs}$. Fig.17 shows these results, expressed in terms of post-improvement $(N_1)_{60cs}$ for soils with different hydraulic conductivities k, for a set of pre-improvement values of $(N_1)_{60cs}$ and A_r. The three figures in the first row (Fig.17a) represent soils with pre-improvement $(N_1)_{60cs}$ of 7, 11 and 16, respectively, improved using A_r =5.6%. The second and third rows (Figs.17b-c) are for soils improved using A_r =10% and 22.5%, respectively. Each figure has two curves, one for improvement with stone columns only, and the other for improvement by stone columns supplemented with pre-installed wick drains.

Results indicate the following. Stone columns without pre-installed wick drains are effective in improving sands with k values larger than 10^{-5}m/s. Effectiveness of SC diminishes with a decrease in k (or with an increase in silt content). At A_r approaching 22.5% or higher, stone columns may be effective in improving silty soils with k values as low as 10^{-7}m/s, provided that wick drained are pre-installed. The degree of improvement that can be achieved diminishes with a decrease in k (or silt content).

CONCLUSIONS

Non-plastic silt content in silty sands affects liquefaction resistance, cone penetration resistance and soil response during ground improvement using dynamic compaction and stone columns in different ways. For liquefaction, silt content affects the intergrain contact density of the soil compared to that of a sand at the same void ratio. When this is taken into account, sand and silty sand show similar liquefaction resistance at the same equivalent void ratio $(e_c)_{eq}$. Silt content also significantly affect the hydraulic conductivity k and coefficient of consolidation c_v in silty soils compared to sand. Cone resistance is sensitive to $(e_c)_{eq}$ as well as k and c_v. It appears that normalized cone resistance q_{c1N} may be correlated with equivalent relative density and a parameter T (=vd/c_v) that represents c_v, cone diameter d and penetration speed v. There is likely a correlation possible between liquefaction resistance, q_{c1N} and T.

Low hydraulic conductivity and c_v for silty soils appear to adversely affect soil densification process during dynamic compaction and stone column installation. Pre-installation of closely spaced wick drains appear to expedite dissipation of excess pore pressures during DC and SC installation and enhance soil densification. In both cases, silty soils with k values as low as 10^{-7}m/s may be effectively improved using DC and SC, with preinstalled wick drains, for liquefaction mitigation.

Additional field test data are needed to further verify and refine these findings.

ACKNOWLEDGMENT

Financial support for this research was provided by National Science Foundation, and USGS NEHRP program, and MCEER Highway Project 094, sponsored by the Federal Highway Administration. This assistance is greatly appreciated. T. Shenthan, R. Nashed, N. Ecemis, Y. Liang, T. Kanagalingam and Q. Huang are thanked for their assistance in this work.

REFERENCES

ABAQUS, [2000]. User's manual, Hibbitt, Karlsson & Sorensen, Inc., Fremont, CA.

Andrus, R. D. and Stokoe, K. H. [2000] "Liquefaction resistance of soils from shear-wave velocity", *J. Geotech. and Geoenv. Eng., ASCE*, Vol.126(11), 1015-25

ASTM [1993] "Designation D3441 – Standard test method for deep quasi-static, cone, and friction cone penetration tests of soil. In soil and rock: Building Stones" *Annual Book of ASTM Standards*, Vol. 4.08, American Society for Testing and Materials, Philedalphia, PA

Baez, J.I. [1995]. "*A design model for the reduction of soil liquefaction by vibro-stone columns*" Ph.D. Dissertation, USC, Los Angeles, CA. 207 p.

Berrill, J.B. and Davis, R.O. [1985]. "Energy dissipation and seismic liquefaction in sands: Revised model." *Soils and Found*., Tokyo, 25(2), 106-118.

Castro, G. [1975] "Liquefaction and cyclic mobility of saturated sands", *J. Geotech. Eng. Div., ASCE*, Vol. 101(6), 551-569.

Chang, N. Y., Yeh, S. T., and Kaufman, L. P. [1982] "Liquefaction potential of clean and silty sands" *Proc., 3rd Int. Earthquake Microzonation Conf.*, Vol. 2, 1017-1032

Dise, K., Stevens, M.G., and Von Thun, J.L. [1994]. "Dynamic compaction to remediate liquefiable embankment foundation soils", ASCE, *Geotech. sp. pub.*, No. 45, pp.1-25.

Ecemis, N. [2008]. "*Effects of soil permeability and compressibility on liquefaction screening using cone penetration resistance*", Ph.D. Dissertation, University at Buffalo, Buffalo, NY.

Figueroa, J.L., Saada, A.S., Liang, L., and Dahisaria, M. N. [1994]. "Evaluation of soil liquefaction by energy principles." *ASCE, J. Geotech. Eng*., 120(9),1554-1569.

FWHA [200]). "*Stone columns*" Ground Improvement Technical Summaries, II, Publication No. FHWA-SA-98-086R: (7-) 1-84.

Green, R. and Mitchell, J. K. [2004]. "Energy-based evaluation and remediation of liquefiable soils", *Proc. Geotech. Eng. for transportation projects, ASCE*, 1961-1970

Han, J. [1998] "Ground modification by a combination of dynamic compaction, consolidation, and replacement" *Proc. 4th Int. Conf. on case histories in geotechnical Engineering*, St. Louis, Missouri, 1998, pp. 341-346.

Kayen, R.E. and Mitchell, J.K. [1997]. "Assessment of liquefaction potential during earthquakes by arias intensity." *ASCE, J. Geotech. & Geoenv. Eng.*, 123(12), 1162-1174.

Koester, J. P. [1994] "The influence of fines type and content on cyclic resistance" *Ground Failures under seismic conditions, Geotech Spec. Publ.* No. 44, ASCE, New York, 17-33.

Kuerbis, R., Negussey, D., and Vaid, V. P. [1988] "Effect of gradation and fines content on the undrained response of sand" *Proc., Hydr. Fill Struct.*, 330-345

Luehring, R., N. Snorteland, L. Mejia, and Stevens, M. [2001]. "Liquefaction mitigation of a silty dam foundation using vibro-stone columns and drainage wicks: a case history at salmon lake dam", *Proc. 21st USSD annual meeting and lecture*, Denver, CO.

Lukas, R.G. [1995] "*Dynamic compaction*", Federal Highway Admin., Rep. FHWA-SA-95-037.

Nashed, R. [2006] *Liquefaction mitigation in silty soils using dynamic compaction*. PhD Dissertation, State University of New York at Buffalo, Buffalo

Nashed, R., Thevanayagam, S., and Martin, G. R. [2009a] "Densification and Liquefaction Mitigation of Saturated Silty Soils by Dynamic Compaction – Design" *Ground Improvement Journal* 162(G12), Institute of Civil Engineers, UK, p69-80.

Nashed, R., Thevanayagam, S., and Martin, G. R. [2009b] "Densification and Liquefaction Mitigation of Saturated Silty Soils by Dynamic Compaction – Numerical Simulation", *Ground Improvement Journal*, 162(G12), Institute of Civil Engineers, UK. p81-91.

Ni, Q., Tan, T. S., Dasari, G.R., and Hight, D.W. [2004] "Contribution of fines to the compressive strength of mixed soils" *Geotechnique*, Vol. 54(9), 561-569

Polito, C. P. and Martin II, J. R. [2001] “Effects of nonplastic fines on the liquefaction resistance of sands” *J. Geotech. and Geoenv. Eng. Div., ASCE*, Vol. 127(5), 408-415

Robertson, P.K. and Wride, C.E. [1997] “Evaluation of cyclic liquefaction potential based on the CPT”, *Seis. Behavior of Ground & Geotech Struct., Balkema Publs.*, 269-278.

Seed, H. B., Martin, G. R., and Pyke, C. K. [1978] “Effects of multi-directional shaking on pore pressure development in sands”, *J. Geotech. Eng. Div., ASCE*, Vol. 104(1), 27-44.

Seed, H. B., Idriss, I. M, and Arango, I. [1983] “Evaluation of liquefaction potential using field performance data”, *J. Geotech. Eng., ASCE*, 109(3), 458-482

Shenthan, T. [2006] *Liquefaction mitigation in silty soils using composite stone columns*. PhD Dissertation, State University of New York at Buffalo, Buffalo.

Thevanayagam, S., Liang, J., and Shenthan, T. [2000]. "A contact index for liquefaction potential analysis of silty/gravely soils." *EM2000, Proc. 14th ASCE EMD Spec. Conf.*, Tassoulas, ed., Austin, Texas.

Thevanayagam, S. Martin, G.R, Shenthan, T. and Liang J. [2001] “Post-liquefaction pore pressure dissipation and densification in silty soils”, *Proc.,4th Intl. Conf. Recent Adv. Geot. Earthq. Eng. & Soil Dyn.*, ed. S. Prakash, Paper# 4.28.

Thevanayagam, S. and Liang, J. [2001] “Shear wave velocity relations for silty and gravely soils”, *Proc. 4th Intl. Conf. Soil Dynamics & earthq. Eng*., San Diego.

Thevanayagam, S., Shenthan, T., Mohan, S. and Liang, J. [2002], “Undrained fragility of sands, silty sands and silt”, *ASCE, J. Geotech. & Geoenv. Eng.*, 128 (10), 849-859.

Thevanayagam, S. and Martin, G. R. [2002] “Liquefaction in silty soils - screening and remediation issues”, *Soil Dyn. and Earthq. Eng.*, 22, 1034-1042.

Thevanayagam, S., Shenthan, T., and Kanagalingam, T., [2003]. “Role of intergranular contacts on mechanisms causing liquefaction and slope failures in silty sands” *Final Report, USGS Award No. 01HQGR0032 and 99HQGR0021, US Geological Survey, Department of Interior, USA*, http://erp-eb.er.usgs.gov/reports/abstract/2001/pt/01hqgr0032-report.pdf, 396p.

Thevanayagam, S., Nashed, R., Shenthan, T., and Martin, G.R. [2006] *Liquefaction mitigation in silty soils using dynamic compaction and stone columns: Design guidelines*, Federal Highway Administration, Technical report MCEER-06-0009, 2006.

Thevanayagam, S. [2007a] “Intergrain contact density indices for granular mixes–I: Framework”, *J. Earthquake Eng. and Eng. Vibrations*, Vol.6 (2), 123-134.

Thevanayagam, S. [2007b] “Intergrain contact density indices for granular mixes–II: Liquefaction resistance”, *J. Earthquake Eng. and Eng. Vibrations*, Vol.6 (2), 135-146.

Thevanayagam, S. and Ecemis, N. [2008] “Effects of permeability on liquefaction resistance and cone resistance”, *ASCE Geotechnical Special Publication 181, Geotechnical Earthquake Engineering and Soil Dynamics*, 11p.

Thevanayagam, S., Nashed, R., and Martin, G. R. [2009] “Densification and Liquefaction Mitigation of Saturated of Silty Soils by Dynamic Compaction – Theory”, *Ground Improvement Journal*, 162(G12), Institute of Civil Engineers, UK. p57-68

Vaid, V. P. [1994], “Liquefaction of silty soils” *Gound failures under seismic conditions, Geotech. Spec. Publ.*, No.44, ASCE, New York, 1-16.

Youd, T. L. and Idriss, I. M. [2001] “Liquefaction resistance of soils: Summary report from the 1996 NCEER and 1998 NCEER/NSF workshops on evaluation of liquefaction resistance of soils.” *J. Geotech. and Geoenv. Eng.*, Vol. 127(4), 297-313

Zlatovic, S. and Ishihara, K. [1997] “Normalized behavior of very loose non-plastic soils: Effects of fabric”, *Soils and Foundations*, Tokyo, Vol. 37(4), 47-56.